

MOTION CORRECTION FOR AUGMENTED FLUOROSCOPY – APPLICATION TO LIVER EMBOLIZATION

James C. Ross¹, Navneeth Subramanian², Stephen B. Solomon³

¹GE Global Research, Niskayuna, NY 12309, USA

²GE Global Research, Bangalore, Karnataka 560066, IN

³Memorial Sloan Kettering Cancer Center, New York, NY 10065, USA

ABSTRACT

Hepatic embolization is a procedure designed to cut off blood supply to liver tumors, either hepatocellular carcinomas (HCC) or metastases from other parts of the body. While it often serves as a palliative treatment, it can also be indicated as a precursor to liver resection and liver transplants. The procedure itself is conducted under fluoroscopic X-ray guidance. Contrast agent is administered to opacify the vasculature and to indicate the arterial branches that feed the treatment target. These supply routes are then blocked by embolic agents, cutting off the tumor's blood supply. While methods exist to enhance fluoroscopic images and reduce the dependency on contrast agent, they are typically confounded by patient respiratory motion and are hence not effective for abdominal interventions. This paper presents an appearance based tracking algorithm that quickly and accurately compensates for the liver's bulk motion due to respiration, thereby enabling the application of fluoroscopic augmentations (i.e. image overlays) for hepatic embolization procedures. To quantify the accuracy of our algorithm, we manually identified vascular and artificial landmarks in fluoroscopy sequences acquired from three patients during free breathing. The average postmotion compensation landmark misalignment was 1.9 mm, with the maximum landmark misalignment not exceeding 5.5 mm.

Index Terms— Liver, motion compensation

1. INTRODUCTION

Liver embolization is a standard method for treating hepatocellular carcinomas (HCC) and liver metastases originating from other parts of the body. Treatment involves threading a catheter to the site of the the tumor using x-ray fluoroscopic guidance. Contrast agent is administered at various timepoints during the procedure in order to opacify the vasculature, making it visible. Once the arterial structures feeding the tumor are identified and the catheter is maneuvered to the proper delivery sites, embolization agent is deployed to selectively block bloodflow to the tumor.

The procedure is complicated by several factors. Contrast agent toxicity limits the number of times that the arteries can

be opacified. This necessitates periodic guidance in fluoroscopic imaging mode in the absence of contrast. Methods to reduce contrast agent burden while simultaneously indicating vascular structure include roadmapping and augmented fluoroscopy [1], a technique to augment fluoroscopy images with vessel structures segmented from a pre-operative 3D dataset (CT/X-ray spin). However, even with the assistance of these methods, respiratory induced liver motion introduces large changes in target position during the embolization, requiring the clinician to continuously estimate target location.

In this paper, we present a method to compensate for respiratory induced liver motion on the fluoroscopy images. Such a system allows for an augmented fluoroscopy set-up, where the pre-operative vascular detail can move in tandem with respiratory induced organ motion manifested on fluoroscopy acquisitions.

Several articles [2, 3] seeking to characterize liver motion have concluded that the respiratory induced liver motion is mostly in the cranio-caudal direction. They report that this motion, in the range of 10-26 mm, is largely translational and that the liver can be approximated as a rigid-body.

We have developed a realtime algorithm that compensates for in-plane liver motion on fluoroscopic X-ray sequences and have conducted studies to investigate the rigid-body approximation of liver motion. In section 2 we describe our motion compensation approach and experiments conducted to validate it. In section 3 we present results and draw conclusions in section 4.

2. METHODS

Gorges et al. [1] describes a technique for improving interventional procedures by augmenting fluoroscopic sequences. Briefly, a 3D C-arm spin dataset is acquired with contrast. From this dataset the contrast-enhanced vascular tree is segmented. The 3D spin acquisition remains in registration with respect to patient location and C-arm orientation, so the segmented vascular tree can be projected onto subsequent fluoro acquisitions given the C-arm system's known projection matrix. This provides interventionalists with views of the pa-



Fig. 1. Pipeline illustrating appearance patch generation. Left: contour defining the lung-diaphragm interface. Center: distance map indicating shortest distance from the contour. Right: appearance patch in the vicinity of the contour.

tient’s vasculature without the need to inject further contrast.

This method has received positive clinical feedback but has only been demonstrated for neuro interventions in which motion is not an issue [4]. In this section, we describe a motion compensation algorithm that enables the application of augmented fluoroscopy for liver embolizations. We also describe a study that we conducted in order to quantify the degree of residual, non-rigid motion not accounted for by our technique.

2.1. Contour Tracking

The first step is to define the appearance patch that is used during the subsequent tracking stage. A single fluoro frame is acquired, and a user manually delineates the lung-diaphragm interface. For this step, we used live-wire [5] to quickly draw the the contour (Figure 1, left).

Once the contour is defined, the Danielsson distance map [6] is automatically computed (Figure 1, center). Each pixel in the distance map indicates the shortest distance to the contour. Because we are only interested in the X-ray intensity values in the vicinity of the contour, we only retain the region that is within a specified distance from the contour. Within this region the intensities of the underlying original frame are used to define the appearance patch. The patch size is important. It should be large enough to lock onto the interface location in each frame, but not so large that spurious features are introduced. A large patch also slows the tracking algorithm by requiring additional computations. We found that setting the distance threshold to ten pixels (4 mm) resulted in both accurate tracking and fast computation. The rightmost image in Figure 1 shows the final appearance patch.

Once the appearance patch has been defined, it is used throughout the procedure as long as the C-arm position and orientation remains constant. If the C-arm moves, the appearance patch must be re-acquired. During subsequent acquisitions the location of the lung-diaphragm interface is found by registering the appearance patch to each frame of the fluoro sequence. To speed the registration we extract a short, one dimensional intensity profile in the cranial caudal direction in the vicinity of the last tracked position. This profile is corre-

lated with a similar intensity profile extracted from the previous frame (centered at the tracked location). The point of maximum correlation indicates where to initialize the patch in the current frame. Once initialized, the tracking algorithm proceeds by registering the appearance patch to the given fluoroscopy frame. Registration is performed using a translation transform, so that rigid in-plane motion (both cranial-caudal and left-right) is compensated for.

We implemented our tracking algorithm with the Insight Toolkit (ITK) [7] registration framework using the regular step gradient descent optimizer and the normalized correlation image alignment metric. The task is to find a translation transform that minimizes this metric (1). The metric gives the pixel-wise cross correlation and normalizes it by the square root of the autocorrelation of the images.

$$T = \underset{T}{\operatorname{argmin}} \left\{ -1 \times \frac{\sum_{i \in (T \circ \Omega)} I_i \cdot (T \circ P)_i}{\sqrt{\sum_{i \in (T \circ \Omega)} I_i^2 \cdot \sum_{i \in (T \circ \Omega)} (T \circ P)_i^2}} \right\} \quad (1)$$

Here, T is the translation transform, I is the image in which to track the lung-diaphragm contour, P is the appearance patch, and Ω is the set of appearance patch pixels coordinates in the frame from which the patch was extracted.

2.2. Motion Analysis

The liver behaves approximately as a rigid body [2, 3], but a small degree of residual motion is present after our algorithm has compensated for bulk translational motion. In order to quantify this motion, we selected three sequences from different liver embolization procedures and manually selected corresponding vascular and artificial landmarks (staples) in each frame (Figure 2). Each sequence was acquired during free breathing, and the respective amplitudes of motion in the cranial-caudal direction were 21 mm, 5 mm, and 12 mm.

For all three sequences we translated each frame to compensate for in-plane translational motion using our algorithm. We then selected a reference frame and computed landmark error vectors. A given error vector shows the direction and magnitude that a specific landmark needs to be displaced in order for it to be aligned with the same landmark in the reference frame. Given that translational motion is assumed to be compensated for, we expect to see error vectors with zero magnitude showing that the liver is perfectly rigid and that the translational motion has been perfectly accounted for. Non-zero error-vector magnitude indicates that a) translational motion has not been perfectly accounted for and/or b) the liver is rotating or behaving in a non-rigid manner.

3. RESULTS

To assess the feasibility of using an appearance-based tracking algorithm, we computed metric values as a function of



Fig. 2. Vasculature landmarks in the liver shown on a window-leveled fluoroscopy frame.

patch displacement from the optimal alignment location. Figure 3 shows that the optimization landscape in the vicinity of the appearance patch's optimal location. The penalty value smoothly increases as a function of appearance patch displacement and indicates the feasibility of our algorithm to lock onto the lung-diaphragm interface image feature.

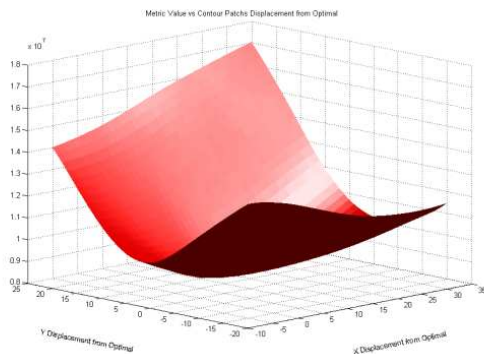


Fig. 3. Metric landscape illustrating smoothly increasing penalty as a function of distance from optimal patch location.

Figure 4 shows error vectors superimposed on the sequence's reference frame as well as a polar plot to indicate landmark misalignment after translational motion correction. Note that the error vectors superimposed on the fluoro frame have been scaled (by a factor of fifteen) for display purposes and are intended to convey the nature of the non-compensated motion field. The polar plot presents quantitative values for this frame's error vectors. Note that the majority of the error vector magnitudes for this frame are below 1 mm, and all of the magnitudes are below 2.5 mm.

Note also that there is a non-zero net error vector. This

indicates that bulk translational motion in this region has not been fully compensated for. Possible causes are slight misregistration of the appearance patch for this frame, liver rotation, or a breakdown in one of our fundamental assumptions: that the motion of the lung-diaphragm interface can be used to fully compensate for the liver's bulk, in-plane translational motion. While we didn't quantitatively attempt to disambiguate these causes, we qualitatively observed that the contour was tracked accurately across all frames considered. Kitamura et al. [8] indicates that the liver exhibits slightly different motion characteristics from lobe to lobe, and this is the likely cause of the systematic bias that we observe. Nevertheless, this bias was not observed in all frames (landmarks were selected in different regions in the three subjects), and the degree of bias, when present, varied throughout the sequence. The example shown here represents a more extreme case and was selected to make this point.

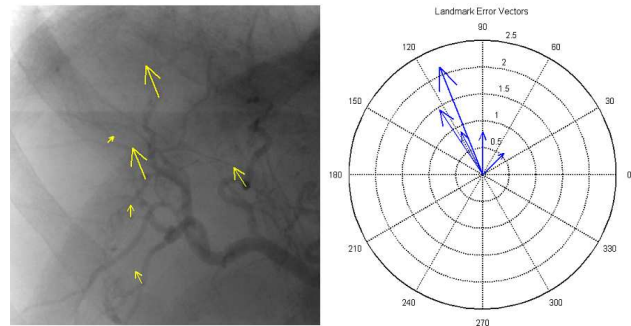


Fig. 4. Left: Landmark error vectors showing residual misalignment after motion compensation (vectors scaled by a factor of fifteen for display purposes). Right: Polar plot summarizing frame's error vectors. All error vectors for this frame are less than 2.5mm in magnitude.

Figure 5 gives a histogram of error vector magnitudes compiled over all three fluoroscopy sequences considered in this study. The majority of the landmarks are registered to within 1.5 mm. Given the range in cranial-caudal motion amplitude of the subjects considered (21 mm, 5 mm, and 12 mm), this is very encouraging. Additionally, figure 6 illustrates a motion corrected vessel tree augmentation on a fluoroscopy frame and also qualitatively shows the areas of misalignment for this frame. Clinical evaluation will determine if this level of alignment is acceptable for fluoroscopy-guided embolization procedures.

Tracking needs to be realtime, as fluoroscopy sequences are acquired with a frame rate of thirty frames or fifteen frames per second. The intensity profile correlation step initializes the patch very close to its optimal location. This minimizes the number of optimizer iterations needed to converge on the best location. Furthermore, the initialization permits small appearance patch sizes which reduces the num-

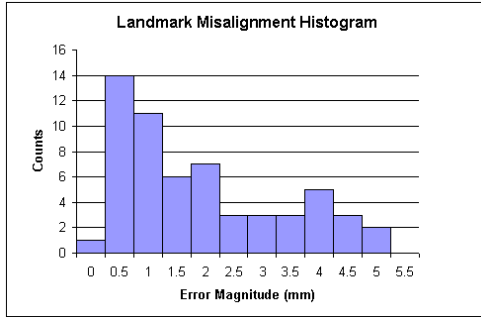


Fig. 5. Histogram of landmark misalignment magnitudes. The majority of landmarks are registered to within 1.5 mm.

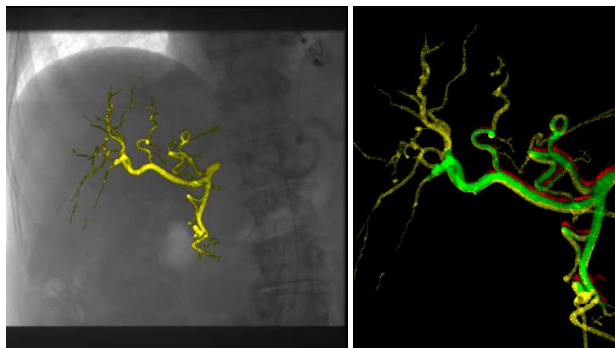


Fig. 6. Left: Vessel tree segmented from one frame, motion corrected, and overlaid on another. Right: yellow – vessel augmentation for the given frame; green – overlap of augmentation and the opacified vessels for that frame; red – mismatch between augmentation and the frame's opacified vessels.

ber of computations per iteration. This approach enables very fast registration speeds: we measured the mean registration time to be 0.032 seconds with a standard deviation of 0.015 seconds – sufficient for realtime application.

4. CONCLUSION

We have presented a realtime algorithm that enables accurate liver motion compensation via lung-diaphragm contour tracking. The method compensates for in-plane translational motion of the liver and can potentially be used to effectively extend augmentations to fluoroscopy-guided liver interventions. We also conducted an accuracy study to determine landmark misalignment post motion compensation. While the algorithm produced alignment results to within approximately 2 mm on average (across test sets with cranial-caudal motion amplitudes of 21 mm, 5 mm, and 12 mm), we need to obtain clinical feedback to understand if this level accuracy is acceptable for interventional liver procedures.

Ultimately, the goal is to provide more efficient means for conducting liver embolizations – by reducing the need for contrast and by reducing the total procedure time. The degree to which our tracking algorithm accomplishes this will be the final measure of its usefulness. Early clinical feedback suggests that vasculature alignment within 2 mm is quite good for embolizations, where the mis-alignment was previously in the range of 2 cm. The need for motion compensation is clear, and we believe our tracking method coupled with dynamic roadmapping or augmented fluoroscopy would provide an improvement upon standard clinical practice.

5. REFERENCES

- [1] Gorges, S., Kerrien, E., Berger, M.O., Trouset, Y., Pescatore, J., Anxionnat, R., Picard, L.: Model of a vascular c-arm for 3d augmented fluoroscopy in interventional radiology. In Duncan, J.S., Gerig, G., eds.: MICCAI (2). Volume 3750 of Lecture Notes in Computer Science., Springer (2005) 214–222
- [2] Clifford, M.A., Banovac, F., Levy, E., Cleary, K.: Assessment of hepatic motion secondary to respiration for computer assisted interventions. *Computer Aided Surgery* (2002) 291–299
- [3] Sears, W.P.: Development and Application of the New Dynamic NURBS-based Cardiac-Torso (NCAT) Phantom. PhD thesis, The University of North Carolina (2001)
- [4] Gorges, S., Kerrien, E., Berger, M.O., Pescatore, J., Trouset, Y., Anxionnat, R., Bracard, S., Picard, L.: 3d augmented fluoroscopy in interventional neuroradiology: precision assessment and first evaluation on clinical cases. In: Workshop AMI-ARCS06 held in conjunction with MICCAI'06, Copenhagen, Denmark (2006)
- [5] Barret, W., Mortensen, E.: Interactive live-wire boundary extraction. *Medical Image Analysis* **1** (1997) 331–341
- [6] Danielsson, P.E.: Euclidean distance mapping. *Computer Graphics and Image Processing* **14** (1980) 227–248
- [7] Ibanez, L., Schroeder, W., Ng, L., Cates, J.: The ITK Software Guide. Kitware, Inc. ISBN 1-930934-15-7, <http://www.itk.org/ItkSoftwareGuide.pdf>. Second edn. (2005)
- [8] Kitamura, K., Shirato, H., Steppenwoolde, Y., Shimizu, T., Kodama, Y., Endo, H., Onimaru, R., Oda, M., Fujita, K., Shimizu, S., Miyasaka, K.: Tumor location, cirrhosis, and surgical history contribute to tumor movement in the liver, as measured during stereotactic irradiation using a real-time tumor tracking radiotherapy system. *Int. J. Radiation Oncology Biol. Phys.* **56** (2003) 221–228